Soft Matter

PAPER

View Article Online
View Journal | View Issue

Cite this: *Soft Matter*, 2017, **13**, 1276

Kinetics of polymer collapse: effect of temperature on cluster growth and aging

Suman Majumder,* Johannes Zierenberg and Wolfhard Janke

Received 27th September 2016,
Accepted 30th December 2016

DOI: 10.1039/c6sm02197b

www.rsc.org/softmatter

Using state of the art Monte Carlo simulations of a bead-spring model we investigate both the equilibrium and the nonequilibrium behavior of the homopolymer collapse. The equilibrium properties obtained *via* multicanonical sampling recover the well-known finite-size scaling behavior of collapse for our model polymer. For the nonequilibrium dynamics we study the collapse by quenching the homopolymer from an expanded coiled state into the globular phase. The sequence of events observed during the collapse is independent of the quench depth. In particular, we focus on finding out universal scaling behaviors related to the growth or coarsening of clusters of monomers, by drawing phenomenological analogies with ordering kinetics. We distinguish the cluster coarsening stage from the initial stage of primary cluster formation. By successful application of a nonequilibrium finite-size scaling analysis we show that at all quench temperatures, during the coarsening stage, the cluster growth is roughly linear and can be characterised by a universal finite-size scaling function. In addition, we provide evidence of aging by constructing a suitable autocorrelation function and its corresponding dynamical power-law scaling with respect to the growing cluster sizes. The predicted theoretical bound for the exponent governing such scaling is strictly obeyed by the numerical data irrespective of the quench temperature. The results and methods presented here in general should find application in similar phenomena such as the collapse of a protein molecule preceding its folding.

1 Introduction

Depending on the solvent condition a polymer chain remains in an expanded state (in a good solvent or at high temperature where the monomer–solvent interaction is stronger) or in a compact globular state (in poor solvent or at low temperature where the monomer–monomer interaction is stronger).[1,2] Hence, when a polymer in an expanded state is suddenly transfered to a poor solvent (or quenched to lower temperatures) it undergoes a coil-globule or collapse transition, and it relaxes towards the globular phase *via* a nonequilibrium pathway. Understanding this phenomenon is of fundamental importance considering its relevance for early stages of protein folding.[3–6] The equilibrium aspect of this transition both from the static and the dynamic point of views, particularly the behavior of a polymer above and below the collapse transition, are well understood.[7–9] In contrast, the understanding of the nonequilibrium aspects, *i.e.*, the kinetics, is still developing.[10–13] Experimental realization of the collapse transition was rare in the past[14–16] due to certain difficulties, *e.g.*, preparing a super dilute solution, finding a long enough polymer with negligible polydispersity, *etc.* However, with recent developments in techniques like small angle X-ray scattering, single molecule fluorescence, and dynamic light scattering it is possible to monitor the collapse of a single molecule.[3–6,17] This has increased the interest to look more into the dynamics of single polymers recently. Another notable feature of the collapse transition is its striking similarity with the phase-ordering or coarsening phenomena of particle systems where nonequilibrium theories are very well developed.[18,19] All these relevant connections with other known phenomena motivate us to understand various nonequilibrium aspects of the collapse transition particularly by drawing analogies with phase-ordering or coarsening kinetics which in turn provides some new insights.

The first and the foremost theory on the dynamics of the collapse transition was proposed by de Gennes in his phenomenological "sausage model"[20] which considers hydrodynamic dissipation of energy during the collapse by minimizing the interfacial energy. Following this, there were a few studies using Monte Carlo (MC) dynamics,[21] Langevin dynamics[22] and Gaussian self-consistent methods[23] without considering hydrodynamic effects. These studies mostly concentrated on the scaling of the collapse time τ_c with the degree of polymerization N resulting in no consensual conclusion. Later Halperin and Goldbart (HG) came up with their "pearl-necklace" model[24] which proposes a step-wise picture of the collapse. According to HG the collapse

Institut für Theoretische Physik, Universität Leipzig, Postfach 100 920, 04009 Leipzig, Germany. E-mail: suman.majumder@itp.uni-leipzig.de, johannes.zierenberg@itp.uni-leipzig.de, wolfhard.janke@itp.uni-leipzig.de

initiates with the formation of small nascent clusters of monomers along the chain. Afterwards these clusters become stable and start growing by withdrawing monomers from the bridges, connecting them. Eventually the bridges stiffen leading to coalescence of connected clusters to form bigger clusters. This continues until all the monomers accumulate to a single cluster. Then, in the final stage of the collapse, the monomers within the single cluster undergo rearrangements to form a compact globule. Along with this description HG also provided scaling laws for the relaxation times of each stage. From a phenomenological point of view the second stage of the collapse bears significant similarities with the coarsening phenomena as observed for Ostwald ripening and other coarsening systems like ordering of ferromagnets. Typically, these are characterized by a length scale $\ell(t)$ which grows with time t in a power-law manner as $\ell(t) \sim t^{\alpha_\ell}$, where the exponent α_ℓ depends on the order-parameter conservation law and the transport mechanism of the system considered.

In case of cluster growth during polymer collapse the relevant length scale is the average linear size (or radius) of the clusters. However, in this work for the sake of comparison with previous studies we will be dealing with the average mass $C_s(t)$, or the average number of monomers in a clusters. Then $C_s(t) \sim \ell(t)^d$ where d is the dimension such that one must expect a scaling of the form

$$C_s(t) \sim t^{\alpha_c}, \tag{1}$$

with $\alpha_c = d\alpha_\ell$ as the corresponding cluster-growth exponent. For a wide variety of systems that have diffusive transport of mass, *e.g.*, vapor–liquid condensation[25] and solid binary mixtures,[18,19,26] the exponent is found to be consistent with the Lifshitz–Slyozov (LS) value of $\alpha_c = 1$.[27] At this point it would be worth mentioning that there are very few studies existing on the collapse of a polymer, where this nonequilibrium phenomenon of cluster growth has been emphasized. In this regard, previous numerical studies based on MC simulations of a lattice polymer[23] report $\alpha_c = 1/2$ and Langevin simulations of a bead-spring model[22] report $\alpha_c = 2/3$, both much lower than the LS value. In presence of hydrodynamics one must expect a much faster growth.

Exploiting the similarities and drawing analogies with the nonequilibrium phenomena of phase-ordering kinetics, suggest also to look at the behavior of the multiple-time quantities which gives information about the presence of aging[28,29] in such processes. One of the major ways of examining aging is by calculating a two-time autocorrelation function $C(t,t_w)$ involving the waiting time t_w and the observation time t, with the former being the age of the system. In the next section we describe the details of measuring $C(t,t_w)$. The absence of time-translational invariance in such functions marks the presence of aging in the evolving system. Particularly, one is interested in the related scaling of the autocorrelation function with respect to the growing nonequilibrium length scale as

$$C(t, t_w) \sim \left[\frac{\ell(t)}{\ell(t_w)}\right]^{-\lambda}, \tag{2}$$

where λ is the dynamic aging exponent. The understanding of such a scaling law is richly developed, especially for ferromagnetic ordering.[28,29] In this regard the top-tier prediction was by Fisher and Huse (FH)[30] about a dimension dependent bound on λ as

$$d/2 \leq \lambda \leq d. \tag{3}$$

Although initially predicted for spin glasses, the validity of this bound for ferromagnetic ordering is confirmed both in theory and simulations.[31,32] There are even attempts to derive the full form of such scaling functions for the ferromagnetic ordering.[32–34] In contrast, aging during collapse of a polymer has rarely been looked upon,[35,36] more precisely the presence of dynamical scaling of the form (2) has only recently been observed.[12]

In this work we thus aim to revisit various kinetic aspects of a homopolymer collapse in a poor solvent. Borrowing the nonequilibrium finite-size scaling tool from phase-ordering kinetics we estimate the exponent of the scaling of cluster growth during the collapse, and show that the scaling is rather independent of the quench depth. In addition, we provide evidence for the presence of aging and corresponding power-law scaling behavior by designing a framework to calculate an analogue of the density–density autocorrelation. Furthermore, we provide a simple scaling argument to derive a bound on the dynamical aging exponent which we validate by comparing with our results from MC simulations.

The remainder of the paper is organized in the following way. We describe the model, methods and observables in Section 2. In Section 3 we present a few basic results from equilibrium studies of the specific model we are considering. Section 4 includes our main results from the nonequilibrium dynamics related to the cluster growth and aging. Finally we present a summary of our results and conclusions in Section 5.

2 Simulation details

2.1 Model

We consider a single bead-spring polymer with N monomers connected successively in a linear chain. The interactions are following ref. 10, 37 and 38: bonded monomers at a distance r apart, interact *via* a finitely extensible nonlinear elastic (FENE) potential

$$V_{\mathrm{FENE}}(r) = -\frac{K}{2}R^2 \ln\left(1 - [(r - r_0)/R]^2\right), \tag{4}$$

with $r_0 = 0.7$, $R = 0.3$, and $K = 40$. Non-bonded monomers interact *via* the standard Lennard-Jones (LJ) potential

$$V_{\mathrm{LJ}}(r) = 4\varepsilon[(\sigma/r)^{12} - (\sigma/r)^6], \tag{5}$$

with the interaction strength $\varepsilon = 1$ and the diameter of the monomers $\sigma = r_0/2^{1/6}$. For numerical reasons and in order to be consistent with the aforementioned literature, the Lennard-Jones potential is cutoff and shifted at $r_c = 2.5\sigma$ such that

$$V_{\mathrm{LJ}}{}^*(r) = \begin{cases} V_{\mathrm{LJ}}(r) - V_{\mathrm{LJ}}(r_c) & r < r_c \\ 0 & \text{else} \end{cases} \tag{6}$$

has the same qualitative behavior and is still continuous at r_c. The unit of temperature (T) in our simulations is ε/k_B where k_B is the Boltzmann constant also set to unity. The LJ potential accounts for excluded volume and short-range attraction, modelling implicit solvent. The polymer undergoes a collapse transition at $T_\theta(N)$ which we determine in the next section *via* equilibrium analyses. We use polymer chains of length N within a very wide range ($4 \leq N \leq 724$) but for the nonequilibrium study we restrict ourselves to relatively long chains ($N > 256$).

2.2 Methods

2.2.1 Equilibrium. In order to study the equilibrium properties of the collapse transition we employ Markov chain Monte Carlo simulations in the multicanonical ensemble.[39–41] This allows us to sample a broad temperature range and to precisely estimate the collapse temperature with a single simulation. To achieve this we replace the canonical Boltzmann factor $\exp(-E/k_BT)$ by a variable weight function $W(E)$. Iterative modification of this weight function of the form $W^{(n+1)}(E) = W^{(n)}(E)/H^{(n)}(E)$ allows tuning the simulation to yield a flat energy histogram $H^{(n)}(E)$.[42] In fact, we restrict our consideration to the conformational (state) space. In this case, the weight function $W(E_p)$ is defined on a discretized potential energy space. The simulation may be further accelerated by using parallel multicanonical simulations.[43] Canonical expectation values are obtained by time-series and histogram reweighting.[44]

For the study of equilibrium properties, we may randomly draw Monte Carlo update proposals from a (large) set of moves. These include single-monomer displacement, bond-rotation, and double-bridging moves. Additionally, we increase the acceptance rate by employing energy-dependent update ranges. These are implemented such that detailed balance is fulfilled.[45] Statistical errors are estimated by the Jackknife error analysis.[46,47] We restrict the energy range to $[-2N, 0.7N]$ to focus on the collapse transition. In total, we perform 1.28 million measurements in the production run, distributed onto 64–256 cores. Comparable simulation times in terms of the number of transits over the full energy range for all involved system sizes were ensured by empirically choosing $5N\sqrt{N}$ update steps between measurements.

2.2.2 Nonequilibrium. To investigate the kinetics of the collapse we introduce dynamics in the MC simulations by incorporating only the single-monomer displacement moves. A monomer along the chain is picked randomly and an attempt to displace the monomer within a cubic box of edge lengths $\sigma/10$ is made. This trial position is accepted or rejected according to the standard Metropolis algorithm.[48] This type of local move shall reproduce the Rouse scaling[49] observed for the dynamics of a polymer chain in viscous solvent neglecting the hydrodynamics. One Monte Carlo step (MCS) consists of N such attempted moves which we set as the unit of time t. We prepare initially expanded polymer chains with N monomers at high temperature ($T_h = 10.0$) and then quench it into the globular phase at temperatures $T_q < T_\theta(N)$ (obtained from the equilibrium part of our study). Note that all the results presented subsequently are averaged over at least 300 different initial realizations.

2.3 Calculation of observables

Here we describe the calculations of important quantities which will be used in our study. The first quantity in which we are interested is the squared radius of gyration

$$R_g^2 = \frac{1}{N}\sum_{i=1}^{N}(r_i - r_{cm})^2 \tag{7}$$

where r_{cm} is the center of mass of the polymer. Note that for a polymer in the coiled state $R_g^2 \sim N^{2\nu_F}$ with $\nu_F = 3/5$, in the Flory mean-field approximation, and in the globular state $R_g^2 \sim N^{2/d}$. As R_g^2 essentially measures the size of the polymer chain, measuring R_g^2 provides information on the collapse both in equilibrium and nonequilibrium studies as will be shown later.

As mentioned earlier we study the nonequilibrium dynamics of the collapse by monitoring the average sizes of monomer clusters $C_s(t)$, formed during the collapse. We measure $C_s(t)$ as the average number of monomers present in a cluster that we identify in the following way. First we calculate the total numbers of monomers in the nearest vicinity of the i-th monomer as

$$n_i = \sum_{j=1}^{N}\Theta(r_c - r_{ij}), \tag{8}$$

where r_c is the same cutoff distance used in (6) and Θ is the Heaviside step function. For, $n_i \geq n_{min}$, there is a cluster around the i-th monomer and all those n_i monomers belong to that cluster. The total number of clusters calculated this way may include overcounting, which we remove *via* the corresponding Venn diagram, and thus the actual discrete clusters (k) are identified and the number of monomers m_k within each cluster is determined. Finally the average cluster size is calculated as

$$C_s(t) = \frac{1}{n_c(t)}\sum_{k=1}^{n_c(t)} m_k, \tag{9}$$

where $n_c(t)$ is the total number of discrete clusters at time t. Note that the method is dependent only on one nontrivial choice, which is n_{min}. Later we show that in the long time limit the method is independent for a reasonable choice of n_{min}.

The next important quantity is the two-time autocorrelation function $C(t,t_w)$, needed to probe aging. The definition of $C(t,t_w)$ is given as

$$C(t,t_w) = \langle O_i(t)O_i(t_w)\rangle - \langle O_i(t)\rangle\langle O_i(t_w)\rangle, \tag{10}$$

with $t \geq t_w$ and the $\langle\cdots\rangle$ denotes the thermal averaging. Most significantly the variable O_i in (10) is chosen in such a way that it reflects the nonequilibrium changes happening during the time evolution, *e.g.*, the local magnetization in an ordering ferromagnet, time and space dependent density order parameter

in phase separating fluids, *etc.* In the present case of polymer collapse, however, it is not trivial to choose a time and space dependent order parameter. Nevertheless, we identify the observable O_i as a variable based on the cluster identification method described above. We assign $O_i = \pm 1$ depending on whether the monomer is inside (+1) or outside (−1) a cluster. It is apparent that our cluster identification method is based on the local density around a monomer along the chain. Thus $C(t,t_w)$ calculated using this framework gives an analogue of the usual density–density autocorrelation functions in particle systems.

3 Equilibrium properties of the collapse transition

Before going on to the kinetic aspects of the collapse we briefly examine the equilibrium properties so that we have an idea about the temperature spectrum of the chosen model as well as the equilibrium finite-size scaling. In the past 10 years, there has been an interesting discussion in the literature about the scaling of the equilibrium collapse transition temperature of a single flexible homopolymer. Among others, this problem has been discussed using lattice models[50,51] as well as continuous bead-spring models.[52–54] One usually expects a scaling motivated from polymer solutions in the Flory–Huggins mean-field theory. This leads to the fit ansatz

$$T_\theta(N) - T_\theta = -\frac{a_1}{\sqrt{N}} + \frac{a_2}{N}, \tag{11}$$

where $T_\theta = \lim_{N\to\infty} T_\theta(N)$. This has been shown to correctly describe the finite-size corrections to the collapse transition temperature for interacting self-avoiding walks,[51] the bond-fluctuation model[50] and continuous bead-spring polymers.[54] However, in ref. 52 and 53 the authors claim to observe mean-field predicted logarithmic corrections leading to

$$T_\theta(N) - T_\theta = \frac{A}{\sqrt{N}(\ln N)^{7/11}}. \tag{12}$$

The aforementioned contributions[50,51,54] have shown that this is rather unlikely. One interesting observation is that the numerical verification of (12) in ref. 52 and 53 relied on numerical derivatives of sampled densities of states including smoothening. This indicates that here some caution is necessary. Thus we rely on time-series reweighting which is methodically precise.[44,55]

We focus on the first ansatz (11) in order to characterize the collapse transition of our polymer model. Attempts of fitting to the second ansatz do not show satisfying results. For large temperatures, the polymer is entropy dominated and the radius of gyration scales as a self-avoiding walk with increasing chain length. However, with decreasing temperature the short-range attraction becomes more relevant and the polymer undergoes a continuous collapse transition, forming a more compact globule. This is reflected in a decrease of the radius of gyration and the maximal slope may be associated to the collapse transition temperature. Here, $T_\theta(N)$ is obtained from the peak of the temperature derivative of the squared radius of gyration. The canonical curves are shown in Fig. 1(a) where solid lines are results for histogram reweighting and data points are evaluated with time-series reweighting and error analysis. For larger system sizes, the collapse transition shifts to larger temperatures and the peak height increases.

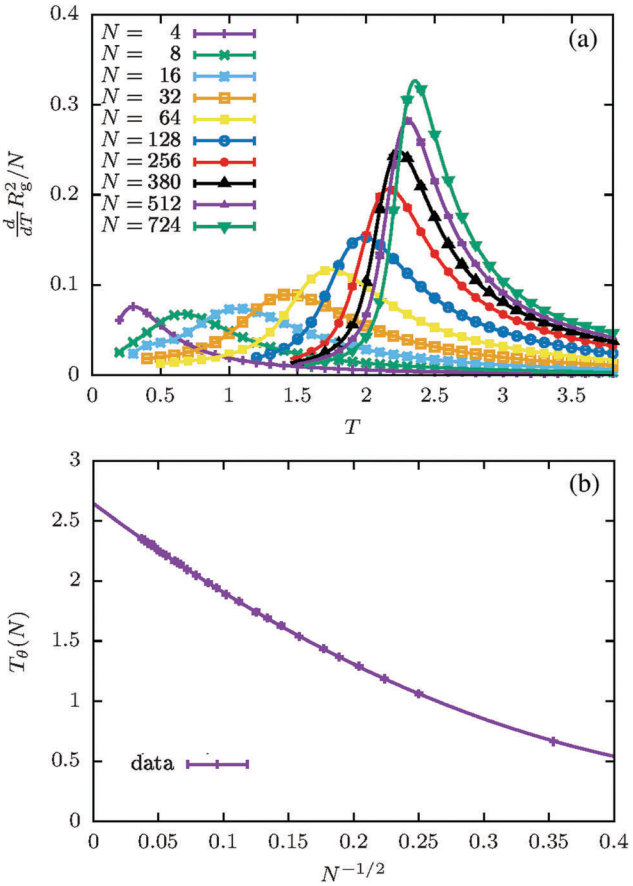

Fig. 1 (a) The canonical temperature derivative of the squared radius of gyration for the bead-spring polymer with non-bonded LJ interaction. (b) Finite-size scaling of the collapse transition temperature. The data is nicely described by the solid line representing the ansatz (11).

The shift in the collapse transition temperature for finite systems is shown in Fig. 1(b), where the data points are plotted against the expected $N^{-1/2}$ scaling behavior. The additional higher-order corrections are clearly visible by the nonlinear behavior in the plot variables. The fit to (11) describes the data points well. For details of the fits and a comparison to a differently parameterized bead-spring polymer[54] as well as a lattice model[51] see Table 1. The differences for both the thermodynamic limit T_θ and finite-size corrections are due to (slightly) different energy (and corresponding temperature) scales from the microscopic details of the models. However, the important result is that all models follow the same finite-size behavior and are thus expected to describe the same generic properties with respect to collapse.[56] For the influence of interaction range on the interplay of collapse and freezing transition see also ref. 57, where the present model is clearly in the second-order regime.

Table 1 Fit results to the scaling Ansatz (11) of the single-polymer collapse transition temperature for different models. The reduced chi-squared χ_r^2 measures the goodness of fit. Our model (fit range $N \in [16, 724]$) and that of ref. 54 are flexible bead-spring models with slightly different parameterizations. The model in ref. 51 is an interactive self-avoiding on a cubic lattice (fit range $N \in [200, 32\,000]$)

Model	T_θ	a_1	a_2	χ_r^2
Our model	2.646(4)	8.11(6)	7.1(2)	≈ 0.2
Ref. 54	3.176(4)	11.56	12.77	
Ref. 51	3.703(6)	32	135	≈ 0.53

4 Nonequilibrium dynamics of the collapse

Having the equilibrium properties of our model polymer in place we move on to the nonequilibrium frontiers, *i.e.*, the kinetics of the collapse. In Fig. 2 we present snapshots showing the evolution of a polymer with $N = 512$ during the collapse for three different quench temperatures T_q well below $T_\theta(512) = 2.31(2)$. The sequence of events observed during the collapse at all T_q is more or less in accordance with the phenomenological "pearl-necklace" picture of HG.[24] The collapse starts with the rapid formation of primary clusters of monomers arising from the density fluctuations along the chain. Afterwards the stable clusters start to diffuse along the chain by withdrawing monomers from the bridges connecting them, eventually leading to the coalescence of clusters to form bigger clusters. The above event keeps on repeating until a single cluster or globule is formed. This particular stage of coalescence and subsequent growth of clusters of monomers during the collapse bears phenomenological similarities with known coarsening phenomena for particle systems. Even though from the snapshots the overall picture for all T_q looks pretty similar, the structural dissimilarities due to thermal fluctuations are quite noticeable. This is more evident in the final collapsed states where the sphericity of the globule increases with the decrease of T_q.

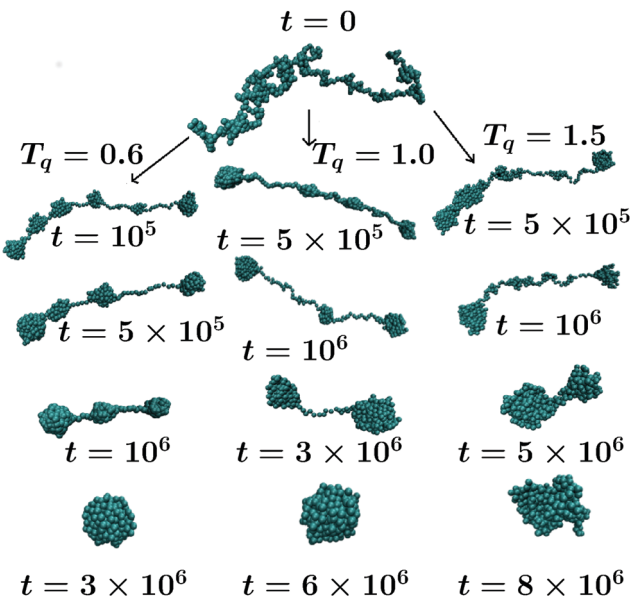

Fig. 2 A comparative picture for the time evolution snapshots of a polymer with $N = 512$ during collapse upon being quenched to three different temperatures $T_q < T_\theta$. For all temperatures the initial condition ($t = 0$) is an extended coil equilibrated at $T_h = 10$.

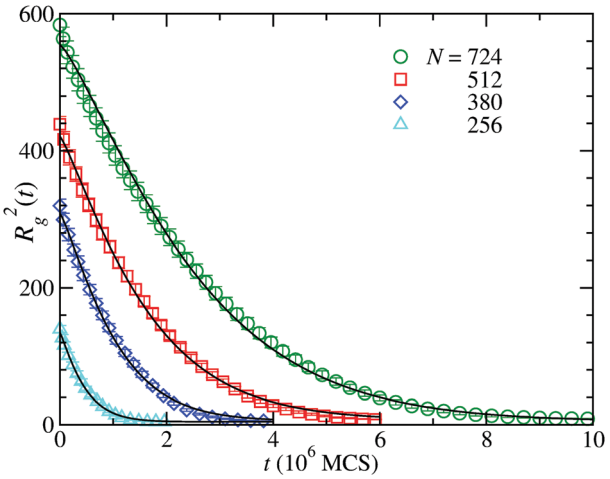

Fig. 3 Variation of the mean squared radius of gyration R_g^2 with time during collapse at $T_q = 1$ for different chain lengths. The solid lines are obtained by fitting the data with the stretched exponential decay (13).

The first "ready to go" way of monitoring the kinetics is to analyze the decay of the mean squared radius of gyration R_g^2 with time. In Fig. 3 we show such plots for different N at $T_q = 1$. Although the decay of $R_g^2(t)$ does not carry stage-wise information about the collapse, it is possible to extract a relaxation time τ_c by fitting the curve with the stretched exponential form

$$R_g^2(t) = b_0 + b_1 \exp[-(t/\tau_c)^\beta], \qquad (13)$$

where b_0 corresponds to the value of $R_g^2(t)$ in the collapsed state, and b_1 and β are associated nontrivial fitting parameters. In Fig. 3 the solid lines are the corresponding best fits using (13) which indeed show nice agreement. Table 2 shows results from this fitting exercise for different N. An exponential fit also works well which can be appreciated from the range of values β obtained. However, for small N, one can observe the monotonic increase in β with N. Even though the form (13) captures the decay of $R_g^2(t)$ pretty well it does not guarantee, however, the exact analytic form. Hence, in addition to the τ_c obtained from the fit we have also extracted the relaxation times τ_{80} and τ_{50}, estimated in a rather crude way. Here, τ_p corresponds to the time when $R_g^2(t)$ has decayed to p% of its total decay, *i.e.*, $\Delta R_g^2 = R_g^2(0) - R_g^2(t \to \infty)$.

Table 2 Results from the fitting of the decay of $R_g^2(t)$ during the collapse with the form (13) for different N at $T_q = 1$

N	b_0	b_1	β	τ_c (MCS)
16	1.14	1.89	0.74	3.24×10^3
32	1.47	5.81	0.91	1.31×10^4
64	2.01	14.95	0.95	3.88×10^4
128	2.92	32.74	1.01	1.01×10^5
256	4.43	133.05	1.27	4.67×10^5
380	4.80	307.10	1.22	1.07×10^6
512	5.20	424.23	1.16	1.69×10^6
724	5.80	552.50	1.18	2.56×10^6

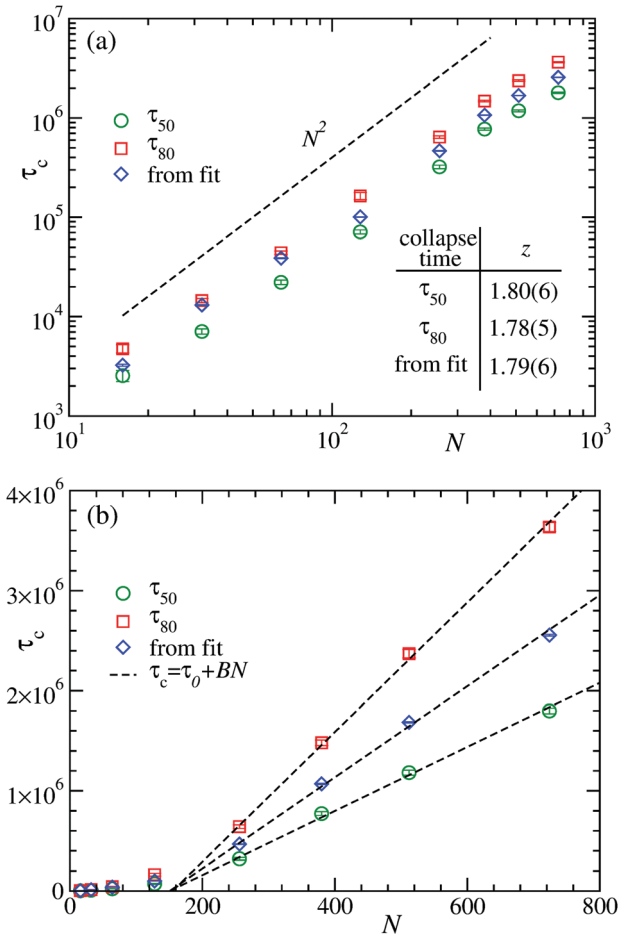

Fig. 4 (a) Scaling of the relaxation times τ_c at T_q = 1, estimated from various methods as described in the text, as a function of the chain length on a double-log scale. The dashed line depicts the Rouse behavior $\tau_c \sim N^2$. The table shows results from fitting the data sets to the form (14). (b) Same as (a) but on a linear scale. The dashed lines show the respective linear fits obtained by using the data for $N > 128$.

In Fig. 4(a) we show the variation of the relaxation times estimated from three different ways as a function of the chain length N. The data on a double-log scale seems to obey the Rouse scaling[49] $\tau_c \sim N^2$ expected for diffusive dynamics, shown by the dashed line. For quantitative purpose traditionally one relies on fitting the data with the form

$$\tau_c = BN^z, \quad (14)$$

where z is the dynamic critical exponent. The results obtained from such fitting are tabulated in Fig. 4(a). It is noteworthy that the value of $z \approx 1.8$ obtained here indicates that the dynamics is faster than observed for lattice polymers[23] albeit slower than a $\tau_c \sim N^{3/2}$ behavior, predicted from a coarse-grained theory of collapse in an off-lattice model.[58] However, our results are comparable with the ones from Brownian dynamics simulations of a bead-spring model.[59] On a different note if the data in Fig. 4(a) are plotted on a linear scale they show apparent linear behavior for $N > 128$, as shown in Fig. 4(b). The dashed lines there are fits to the linear form

$$\tau_c = \tau_0 + BN, \quad (15)$$

where the offset τ_0 can be related to the finite-size correction. The consistency of the data for $N > 128$ with the fitted dashed lines in Fig. 4(b), thus, suggests that a linear scaling of the collapse time τ_c cannot be ruled out at least in the asymptotic limit.

4.1 Cluster-growth kinetics

In this subsection we present results concerning the cluster-growth kinetics, one of the primary objectives of this work. The average number of clusters (n_c) is calculated by the method described in Section 2.3 with n_{min} = 10. In Fig. 5 we show the time dependence of n_c for different N during polymer collapse at T_q = 1. Apparently the curves show a monotonic decrease with time until they attain the value 1, shown by the solid black line. However, an enlarged view of the data at early time reveals that at t = 0 there are very few clusters, merely resulting from the fluctuations in density of monomers along the chain. Initially, there is a stiff rise in $n_c(t)$ to a maximum which then starts decreasing eventually. This indicates that right after the quench there is a rapid formation of a number of primary clusters followed by a gradual crossover to the coarsening stage. To demonstrate the overall consistency of our cluster-identification method we have also plotted the data obtained by using n_{min} = 16 for N = 512 which almost overlap with the data for n_{min} = 10. In the inset of Fig. 5 the mismatch of the data for different n_{min} during the initial cluster-formation stage is noticeable which, however, can be ignored while dealing with the later stage. In the rest of the paper all calculations related to cluster identification have been done using n_{min} = 10.

Before analyzing our results related to scaling of cluster growth we check the presence of any positional preference for the formation and growth of the clusters along the chain. For that we calculate the probability of finding the ith monomer to be within a cluster. In the upper panel of Fig. 6 we show the

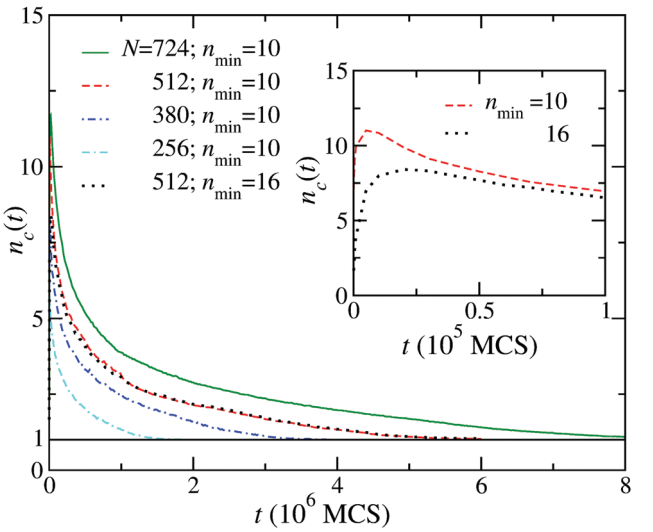

Fig. 5 Variation of the average number of clusters n_c with time during collapse at T_q = 1 for different chain lengths. The inset shows the enlarged data for N = 512 at early times.

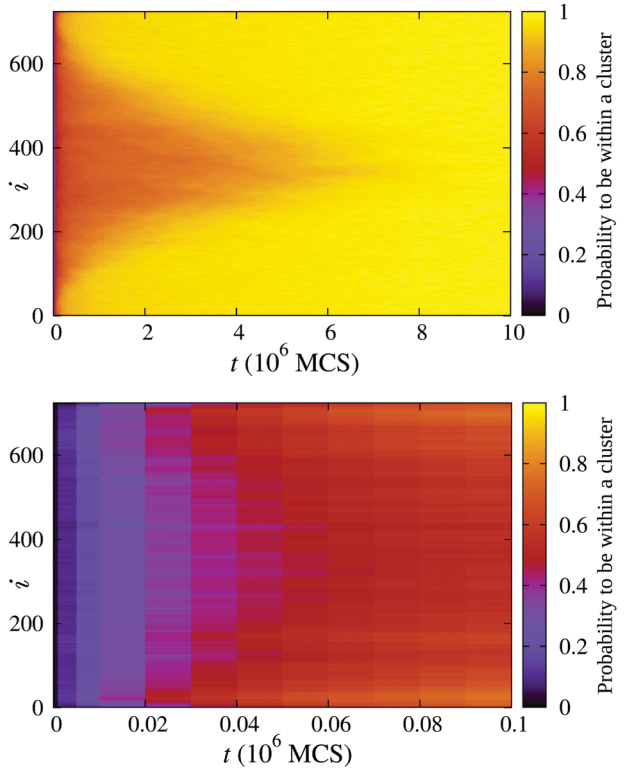

Fig. 6 The upper panel shows the time evolution of the probability of finding a cluster along the length of the polymer with $N = 724$. The lower panel shows the same plot as the upper one but for the initial period ($t \leq 10^5$) of the primary cluster formation.

time evolution of such probability for a polymer of length $N = 724$. Note that here the probability for site i at a particular time measures the fraction of the total number of chains (= 600) we consider for which the ith monomer is within a cluster. The data clearly shows that at intermediate times clusters more preferably reside towards the end of the polymer. At late times the distribution is perfectly uniform due to the fact that all the monomers are by then within a single cluster after the complete collapse ($t > 7 \times 10^6$). However, an enlarged view of the distribution in the early stage ($t \leq 10^5$), shown in the lower panel of Fig. 6, reveals that during this period clusters are formed rather uniformly along the chain with no preference, a feature which is in contrast with a previous observation.[61] In addition this also provides a rough estimate of the crossover time ($t \approx 10^5$) to the coarsening stage. Although rarely considered, such a separation of time scales of the initial cluster-formation stage from the coarsening stage during a nonequilibrium process has recently been observed during condensate formation in driven diffusive systems.[62]

Motivated by the similarities of the cluster coarsening with general coarsening systems we look for the presence of scaling in the morphological properties during collapse. We have calculated the normalized distribution $P(C_d,t)$, *i.e.*, the probability to find a discrete cluster of size C_d among all the clusters at time t. The plots for $P(C_d,t)$ at different times are shown in Fig. 7. These distribution functions are analogous to domain-size distribution

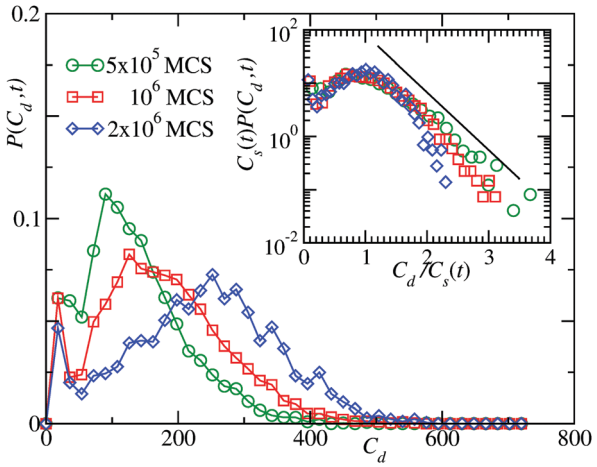

Fig. 7 Normalized distribution of the cluster sizes at three different times during the coarsening stage of the collapse at $T_q = 1$ for a polymer with $N = 724$. The inset shows the semi-log plot of the corresponding scaling of the distribution functions with an exponential tail, as shown to be consistent with the solid black line.

functions used in coarsening phenomena.[26] Following this analogy we look for the presence of scaling[18] of

$$P(C_d,t) \equiv C_s(t)^{-1}\tilde{P}[C_d/C_s(t)], \quad (16)$$

where $\tilde{P}$ is the corresponding scaling function and $C_s(t)$ is the average cluster size which can be calculated as mentioned in Section 2.3 or can be obtained as

$$C_s(t) = \int dC_d C_d P(C_d, t). \quad (17)$$

In the inset of Fig. 7 we show such plots on a semi-log scale which indeed exhibits a reasonable collapse of data. The tail of the curves (in accordance with coarsening in the Ising model[26]) shows an exponential behavior that can be appreciated from consistency of the scaled data with the solid black line. The noisy nature of the data towards the tail is due to lack of statistics and is hard to improve since for a polymer of finite length at later stages of cluster coarsening the total number of clusters is very small.

The scaling of morphology characterizing functions, *e.g.*, two-point equal-time correlation function, structure factor and domain size distribution functions during coarsening in an Ising model suggests the presence of self-similarities in the evolving patterns. This in turn speaks for the presence of a scaling behavior in the growing length scale. Based on this fact, the scaling of cluster-size distribution during the collapse indicates the presence of a scaling of the form (1)

$$C_s(t) = At^{\alpha_c}, \quad (18)$$

where A is a constant. In Fig. 8(a) we plot the average cluster size $C_s(t)$ against time on a linear scale. The data shows an initial nonlinear growth which settles down to an apparent linear growth at intermediate times and then gradually crosses over to the finite-size limit when all the monomers belong to a single cluster. Following the usual trend we plot the data on a

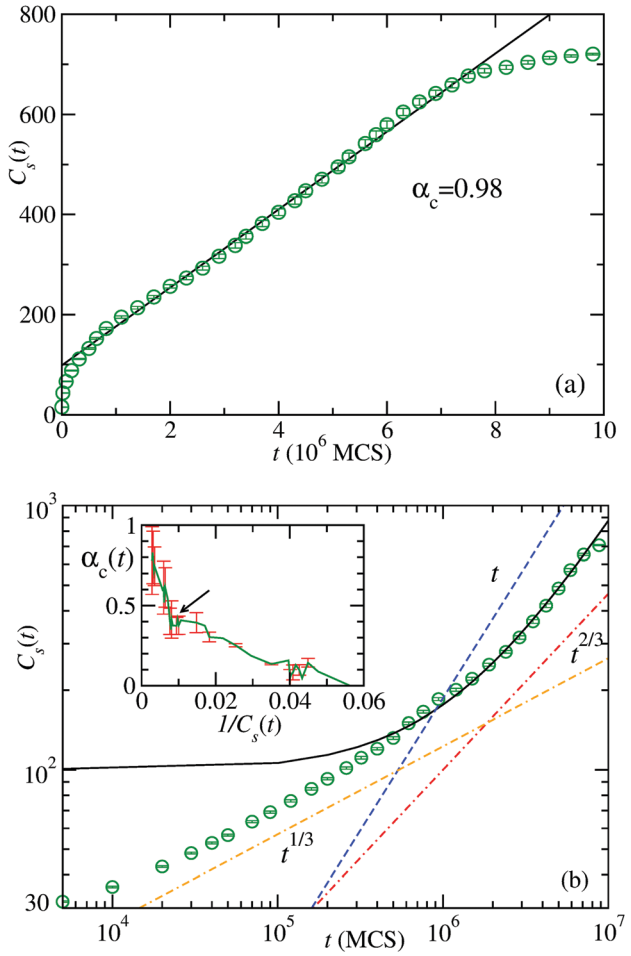

Fig. 8 (a) Growth of the average cluster size $C_s(t)$ with time for a polymer with N = 724 during the collapse at T_q = 1. The solid line is a fit to the form (20). (b) The same data on a double-log scale. The dashed lines there are the expected behaviors as indicated. The inset shows the plot of instantaneous exponent $\alpha_c(t)$ as function of $1/C_s(t)$. Note that the (green) line shows the original data and the error bars (in red) are only put at certain intervals for a clearer view. The arrow there marks the crossover to the coarsening stage.

double-log scale as shown in Fig. 8(b). This signals the crossover from the initial slower growth to the faster growth at late time. The initial regime up to $t \approx t_0 = 5 \times 10^5$ corresponds to the primary cluster-formation stage and the latter to the coarsening stage. The data in the initial stage seem to be fairly consistent with a $t^{1/3}$ behavior shown in the plot. To further distinguish the initial cluster-formation stage from the coarsening stage we calculate the instantaneous exponent[26,60]

$$\alpha_c(t) = \frac{\mathrm{d} \ln C_s(t)}{\ln t}. \tag{19}$$

Following the general practice in the literature,[26,60] in order to see the asymptotic behavior, we plot $\alpha_c(t)$ as a function of $1/C_s(t)$ instead of $1/t$ in the inset of Fig. 8(b). This allows to have a larger window for the late stage such that the data shows a clearer signature of the crossover from an initial slow growth to a faster growth at late times. The late time behavior of $\alpha_c(t)$ indicates that in the asymptotic limit the growth is more likely to be linear. Relying on the form (18), it is, however, unclear from the double-log plot in Fig. 8(b) whether the growth exponent is α_c = 1 (the LS exponent) or α_c = 2/3 as predicted in ref. 21 and 23. In such a case, where a huge offset is present due to a crossover, it is difficult to judge the asymptotic growth exponent using finite systems. Instead it is highly recommended[26] to rely on the form

$$C_s(t) = D + At^{\alpha_c}, \tag{20}$$

where D is a parameter that accounts for the offset. The form (20) successfully captures the cluster growth as shown by the solid line in Fig. 8 obtained as fit yielding α_c = 0.98(2). For details of such fitting exercise we refer to ref. 10. Next we move on to a check of the validity of the form (20) more precisely by performing a nonequilibrium finite-size scaling analysis. In addition to that it allows us to estimate the growth exponent unambiguously.

4.1.1 Finite-size scaling analysis. Finite-size scaling (FSS) analysis was originally introduced in equilibrium critical phenomena[63,64] to tackle the problem of a diverging length scale for a finite system. In an infinite system the singularity of a quantity X around the critical temperature T_c, is quantified in terms of the deviation $|T - T_c|$ as

$$X = X_0|T - T_c|^{-x} \tag{21}$$

where x is the corresponding critical exponent. This holds especially for the divergence of the correlation length ξ as

$$\xi = \xi_0|T - T_c|^{-\nu}, \tag{22}$$

where ν is the related exponent, such that one can rewrite (21) as

$$X = \tilde{X}_0 \xi^{x/\nu} \tag{23}$$

with $\tilde{X}_0 = X_0 \xi_0^{-x/\nu}$. Now, in the critical regime one has $\xi \geq L$ for a finite system with linear dimension L, which allows one to replace ξ with L at T_c to get

$$X = \tilde{X}_0 L^{x/\nu}. \tag{24}$$

More generally, away from T_c where ξ is finite even for $L \to \infty$ by introducing a scaling function $Y(y)$ one can reconstruct (24) as

$$X = Y(y)L^{x/\nu}, \tag{25}$$

where y is a function of the dimensionless scaling variable L/ξ. Note that $Y(y)$ is independent of the system size. Although there is no appropriate understanding of the full form of $Y(y)$ one easily writes down the limiting behaviors. On the one hand, as $|T - T_c| \to 0$ one gets

$$Y(y) = \tilde{X}_0. \tag{26}$$

On the other hand, at $|T - T_c| \gg 0$ for an appropriate choice $y = (L/\xi)^{1/\nu} = |T - T_c|(L/\xi_0)^{1/\nu}$, and by combining (23) and (25) one obtains

$$Y(y) \sim y^{-x} \tag{27}$$

so that (21) and (24) are recovered. Thus by tuning the value of x one looks for the behaviors (26) and (27) along with the optimum collapse of data from different finite systems to extract precisely the numerical value of the exponent x.

Now remembering the results from fitting of the cluster growth we construct the related finite-size scaling ansatz by rewriting (20) as

$$C_s(t) = C_0 + A(t - t_0)^{\alpha_c}, \quad (28)$$

where C_0 is interpreted as the initial crossover cluster size and t_0 is the crossover time from where the coarsening scaling regime starts. While doing FSS analysis it is always preferable to deal only with the scaling part of (28). This is further supported by our exercise where discarding the early time data gives a better fitting result. Hence we identify the analogy with quantities in critical phenomena as $C_s(t) - C_0 \triangleq \xi^d$ and $1/(t - t_0) \triangleq |T - T_c|$. To account for the finite-size effect we now introduce the scaling function $Y(y)$ in (28) and by rearranging it to deal only with the scaling part we write down

$$C_s(t) - C_0 = (N - C_0)\,Y(y), \quad i.e., \; Y(y) = \frac{C_s(t) - C_0}{N - C_0}. \quad (29)$$

In accordance with the choice of y during such FSS analyses for ordering in Ising model[65] we make the judicial choice of the scaling variable

$$y = \frac{(N - C_0)^{1/\alpha_c}}{(t - t_0)}. \quad (30)$$

To recover the finite-size unaffected scaling regime (28) one must have

$$Y(y) \sim y^{-\alpha_c}, \quad (31)$$

and in the finite-size limit when $y \to 0$ one gets $Y(y) \to 1$.

Following the above discussion, we first obtained data for different chain lengths N as shown in Fig. 9(a). The data for smaller N almost follow the data of the larger ones until they get flat. This flattening tendency of the data towards the end marks the onset of finite-size effects when all the monomers accumulate into a single cluster. We use this set of data to do the FSS analysis. By fixing the value of $\alpha_c = 2/3$ and 1 we compare the obtained data collapse, and the corresponding scaling of the master curve. At this point it is worth mentioning that the choice of the range of data or rather the choice of t_0 for FSS analysis plays an important role to obtain the best data collapse. It is known[10] that one has to exclude the initial primary cluster-formation stage, otherwise for $t_0 = 0$ one does not get a collapse of data. Thus based on our fitting exercise we make the convenient choice of $t_0 = 5 \times 10^5$ and use the same for all N to keep the consistency. The corresponding C_0 values are 130, 110 and 100 for $N = 724$, 512, and 380, respectively. The choice of t_0 can further be appreciated from the crossover time that one could roughly extract from the inset in Fig. 8(b), marked by the arrow. In Fig. 9(b) and (c) we show the plots from our FSS analysis. Although both the data show more or less a linear behavior on a double-log scale, the data for $\alpha_c = 1$ in Fig. 9(c) show comparatively a better data collapse than the data for $\alpha_c = 2/3$ in Fig. 9(b). On the one hand, the data for $\alpha_c = 2/3$, shown in Fig. 9(b), has a much steeper slope than the expected $y^{-\alpha_c}$ which implies that indeed the growth exponent is larger than 2/3. On the other hand, the data for $\alpha_c = 1$ in Fig. 9(c) is much more consistent with the expected scaling behavior of $y^{-\alpha_c}$. This confirms the presence of a nearly linear cluster growth during the collapse. The tendency of saturation of the data to 1 for $y \to 0$ is consistent with the finite-size limiting behavior of $Y(y)$ as discussed above. We have tried different values of t_0 and corresponding C_0 in our FSS exercise with no difference in the overall behavior as shown here. As a corollary of the above FSS exercise, from the point of onset of finite-size limiting behavior of $Y(y)$ one can read off the scaling of the characteristic time scale τ_c from (30). This gives $\tau_c \simeq (N - C_0)^{1/\alpha_c} \approx N^{1/\alpha_c}$, for large N, satisfying $C_s(\tau_c) \approx N$. Inserting $\alpha_c = 2/3$ one gets $\tau_c \sim N^{3/2}$ which would be comparable with the behavior observed in Fig. 4(a). However, going with the FSS exercise, if one inserts $\alpha_c = 1$, then it provides $\tau_c \sim N$. This proposition is in accordance with the linear nature of τ_c for $N > 128$, presented in Fig. 4(b).

4.1.2 Temperature dependence of cluster growth. All the analyses carried out so far dealt with a fixed quench temperature $T_q = 1$. Here we look at the effect of the quench temperature T_q on the cluster growth. In our model, changing the temperature mimics the change of the solvent quality. The lower the temperature, the poorer the solvent quality. In Fig. 10 we show kinetics of cluster growth at different T_q. The first noticeable

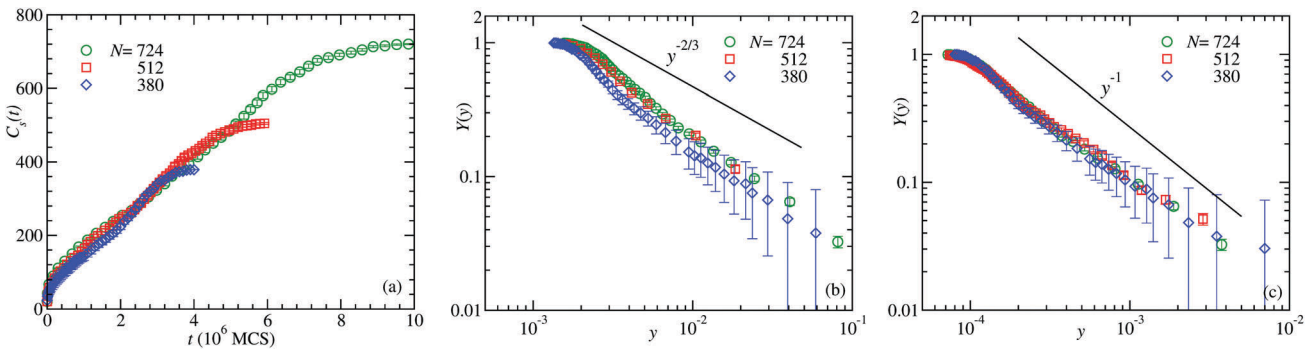

Fig. 9 (a) Plot of cluster growth at $T_q = 1$ for different chain lengths N, as given in the legend. Corresponding plots for finite-size scaling analyses with (b) $\alpha_c = 2/3$ and (c) $\alpha_c = 1$. The solid lines in (b) and (c) show the expected scaling behavior of $y^{-\alpha_c}$.

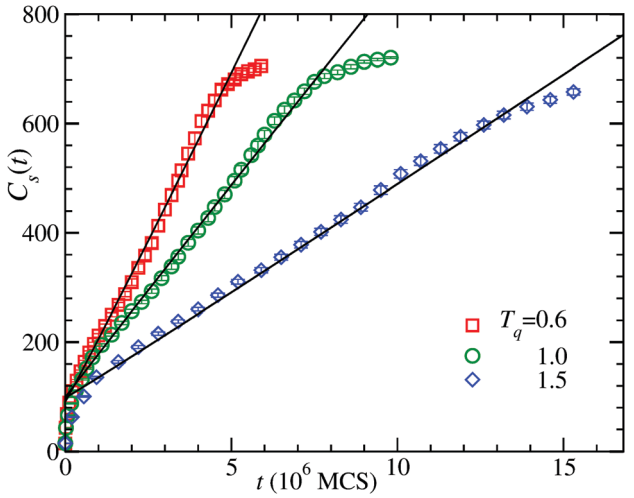

Fig. 10 Plot of average cluster sizes *vs.* time for collapse of a polymer with N = 724 at three different quench temperatures T_q as mentioned. The solid lines are fits to the form (28).

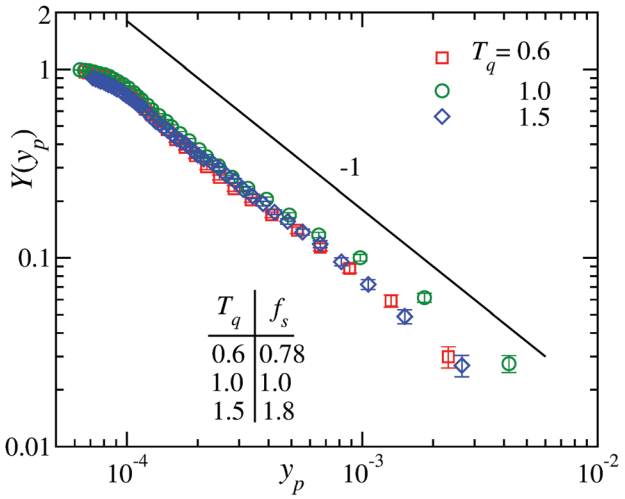

Fig. 11 Double-log plot showing that the cluster growth during the collapse with N = 724 at different quench temperatures can be scaled to a universal finite-size scaling function. The solid line shows the expected power-law behavior of the master curve. The respective values of the used multiplying factor f_s in the scaling variable y_p are mentioned in the table.

information that one draws from the data is that for lower temperature we observe a faster growth. In other words it can be inferred that poorer solvent quality yields faster collapse of the chain. This is in agreement with a previous study by Polson and Zuckermann[66] where they considered explicit solvent and controlled the quality of the solvent by tuning the interaction between the monomers and the solvent molecules. Note that we have chosen the temperatures within the range [0.6,1.5] in order to avoid freezing (for $T_q < 0.5$) or close proximity of T_θ (for $T_q > 1.5$). This should be appreciated by remembering the equilibrium results for our model presented in Section 3.

In Fig. 10 the solid lines are fits to the form (28) but with a temperature (or nature of the solvent) dependent amplitude $A(T_q)$. Note that for different T_q the appropriate values of t_0 would be different as is the case for the time t_f when finite-size effects creep in. The best fitted results obtained for the polymer with N = 724 are tabulated in Table 3. The range of fitting is $[t_0, t_f]$. For all three T_q the value of the growth exponent α_c obtained more or less suggests that the linear cluster growth is independent of temperature. The approximately same values of C_0 obtained for the best fit at different T_q imply that this initial crossover cluster size C_0 is indeed independent of temperature and could be considered as the stable cluster size formed during the initial cluster-formation stage of the collapse.

To add more to this temperature independent scaling of cluster growth we use a treatment analogous to the finite-size scaling, *i.e.*, by using the ansatz (28) as in the previous subsection

Table 3 Results from the fitting of the average cluster size $C_s(t)$ *vs.* t with form (28) for the N = 724 data obtained at different quench temperatures. The reduced chi-squared χ_r^2 indicates the goodness of fit

T_q	t_0 (10^5)	t_f (10^6)	C_0	$A(T_q)$ (10^{-5})	α_c	χ_r^2
0.6	3.0	5.0	129(1)	9.2(1.8)	1.02(3)	1.91
1.0	5.0	8.0	136(1)	6.70(71)	1.01(4)	2.12
1.5	9.0	14.0	135(2)	5.41(71)	0.98(4)	1.51

for the data obtained at different T_q. In doing so we now modify the scaling variable y and rewrite it as

$$y_p = f_s(N - C_0)^{1/\alpha_c}/(t - t_0), \quad (32)$$

where

$$f_s = \left(\frac{A(T_q = 1.0)}{A(T_q)}\right)^{1/\alpha_c} \quad (33)$$

is used to adjust the non-universal amplitudes $A(T_q)$ at different T_q. This allows $Y(y_p)$ obtained from different T_q to collapse onto a master curve showing a power-law decay as a function of y_p with an exponent α_c. To do this exercise we use the data shown in Fig. 10 (N = 724, different T_q). We tune the value of α_c and f_s to obtain the optimum collapse of data by using the C_0 and t_0 from Table 3. For α_c = 0.98(4) we obtain a reasonably good collapse of data. In Fig. 11 we show a representative of such plots where we have used α_c = 1. The collapsed data is reasonably consistent with the expected behavior (31) shown by the solid line, and thus confirming the presence of nearly a linear cluster growth at all T_q. Note that the values of f_s at different T_q, used to obtain the data collapse in Fig. 11, are comparable with the corresponding values one obtains from Table 3. The presence of such a master-curve behavior differing only by a factor in the scaling variable for data at different T_q suggests that the corresponding finite-size scaling function is rather universal. This observation is analogous to the presence of universality of finite-size scaling functions with a non-universal metric factor[67] in critical phenomena of various models or lattices[68] and could be useful for analyses of dynamical scaling of phase-ordering kinetics in other systems, too.

4.2 Aging and related scaling

So far we have investigated the nonequilibrium kinetics of polymer collapse with respect to the cluster growth and related scaling

dealing only with equal-time quantities. Next we move on to another important aspect of the nonequilibrium dynamics namely aging, where one deals with multiple-time quantities. Recall Section 2.3 for the definition and detailed description for calculation of the two-time autocorrelation function $C(t,t_w)$ during polymer collapse based on the cluster identification technique.

In Fig. 12, the main frames show plots of such autocorrelations $C(t,t_w)$ as function of $t - t_w$, at different T_q. For all the cases there is absence of time-translational invariance, indicating the presence of aging irrespective of the temperature. Of course one could easily extract relaxation times associated with the decay for different t_w to provide a quantitative argument about the fact that the higher the age (t_w) the slower is the decay. Note that one could also look for the presence of special aging with $C(t,t_w) \sim t/t_w^{\mu}$, where μ is a nontrivial exponent and $\mu > 1$ (or <1) refers to super (or sub) aging.[35,69] In the present case for all T_q we have checked for the presence of such special aging but in vain, which implies that for the collapse transition the aging is rather simple with $\mu = 1$. In the insets of Fig. 12 we show such scaling of $C(t,t_w)$ with respect to t/t_w on a double-log scale. The consistency of the data for all T_q with the solid line having the slope -0.5 already indicates that the scaling is independent of T_q. For late time the abrupt decay is due to the onset of finite-size effects and it appears earlier with the increase of t_w.

Before we move on further with the scaling of the autocorrelation function, here we check the presence of non-uniformity in the aging of the monomers along the chain. For this we divide the length of the chain into different quarters each having $N/4$ monomers such that the first quarter contains the first $N/4$ monomers along the chain, the second quarter contains the next $N/4$ and so on. Thus by dividing the chain into quarters we calculate the respective autocorrelation $C(t,t_w)$ in the same way as we have done for the full chain using (10). In Fig. 13(a) and (b) we show such plots for $N = 380$ and 724 with $t_w = 10^3$ at $T_q = 1$. The black curves in the plots show the corresponding $C(t,t_w)$ considering all the monomers. Both the plots clearly show that there is indeed a difference in the behavior for different quarters of the chain, which implies that the end quarters age faster than the intermediate ones. This fact can also be appreciated by looking at the snapshots in Fig. 2 at late times where the end monomers are always inside a cluster. This difference is of symmetric nature along the chain as is evident from the overlap of the first and fourth quarter, and the second and third quarter. However, one can also notice that the difference between the curves actually diminishes with increasing chain length, which in turn implies that for large enough chains ($N \to \infty$) all the curves will overlap with the curve obtained using the full chain. From now on all the autocorrelation functions presented in the paper will be calculated considering all the monomers of the chain.

Having provided evidences for the presence of simple aging we now look for the presence of scaling with respect to the growing length scale in the system, a practice widely followed in the ordering kinetics of ferromagnets[28,29] and binary mixtures[70] using the Ising model. In our case the average cluster size $C_s(t)$ serves the purpose of growing length scale. In Fig. 14 we plot $C(t,t_w)$ as a function of the ratio of cluster sizes $x_c = C_s(t)/C_s(t_w)$

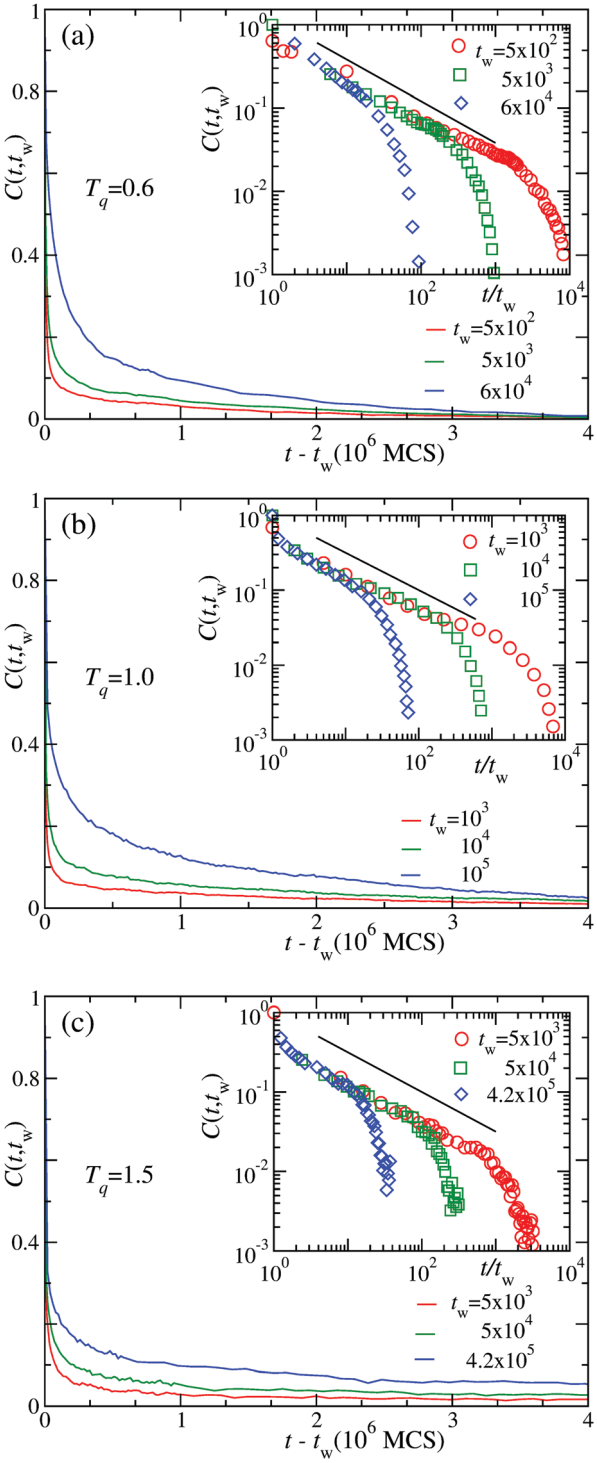

Fig. 12 Autocorrelation function $C(t,t_w)$ as function of the translated time $t - t_w$ for different waiting times as mentioned at three different quench temperatures (a) T_q = 0.6, (b) 1.0, and (c) 1.5, showing the presence of aging during the collapse of a polymer with N = 724. The insets in all the plots show the presence of simple scaling with respect to t/t_w on a double-log scale. The solid lines in all the insets show the power-law behavior having a slope -0.5.

for a polymer with $N = 724$ at $T_q = 1$. The data for different t_w values indeed show nice overlap with each other until they feel the size effects and fall abruptly in the end. The steep early-time

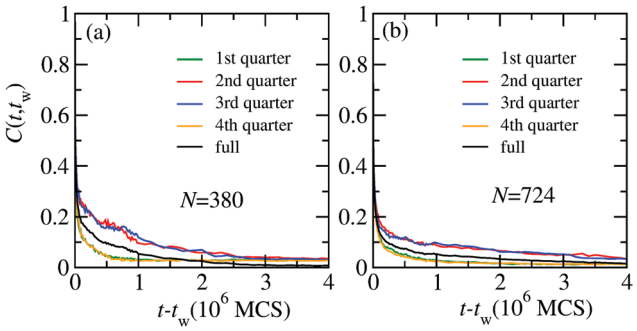

Fig. 13 Autocorrelation function $C(t,t_w)$ *vs.* the translated time $t - t_w$ calculated by considering only the monomers at different quarters along the length of a polymer chain with (a) $N = 380$ and (b) 724 for $t_w = 10^3$ at $T_q = 1$. The black curves show $C(t,t_w)$ calculated using the full chain.

decay is attributed to short-time fluctuations. The linear behavior of the data on a double-log scale suggests that the scaling is a power law in nature which can be quantified as

$$C(t, t_w) = A_c x_c^{-\lambda_c}; \quad x_c = C_s(t)/C_s(t_w), \tag{34}$$

where λ_c is the corresponding aging exponent and A_c is an amplitude that depends on the quench temperature. Below we provide theoretical arguments to derive a bound on this aging exponent λ_c.

Relying on the fact that $C(t,t_w)$ is calculated based on the cluster identification criterion, *i.e.*, by calculating the local monomer densities around each monomer along the polymer chain, it gives an analogue to the usual density–density auto-correlation function as used in glassy systems. Keeping the corresponding argument for the bounds on the respective aging exponent for spin-glass and ferromagnetic ordering[30,31] one can thus assume

$$C(t,t_w) \sim \langle \rho(t)\rho(t_w)\rangle \tag{35}$$

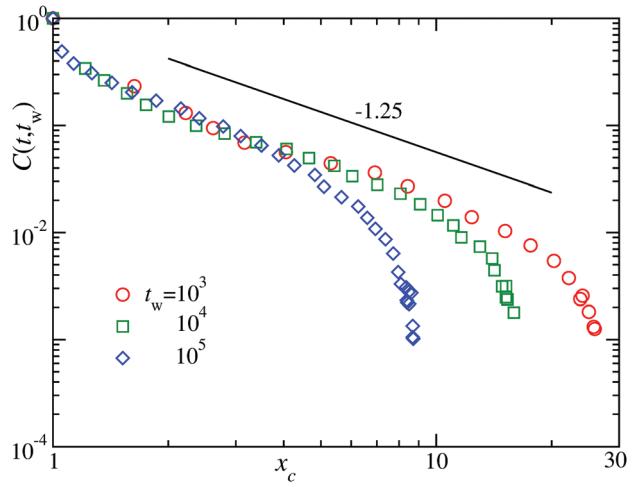

Fig. 14 Plots showing the scaling of the autocorrelation function with respect to the ratio of cluster sizes $x_c = C_s(t)/C_s(t_w)$ for different waiting times t_w for a polymer with $N = 724$ at $T_q = 1$. The solid line with a slope −1.25 shows the consistency of the data with power-law decay (34).

where ρ is the average local density of monomers. Now let us consider a set of C_s monomers at t ($\gg t_w$) and assume that at t_w the polymer is more or less in an expanded coil state where the squared radius of gyration scales as $R_g^2 \sim N^{2\nu_F}$. Using $C_s \equiv N$ in this case one can write

$$\rho(t_w) \sim C_s/R_g^d \sim C_s^{-(\nu_F d-1)}. \tag{36}$$

The above fact can be verified from Fig. 15 where we plot the average geometrical (Euclidean) distance R_e ($\sim R_g$) between the monomers i and j placed at a distance $|i-j|$ along the contour of the chain at different times during the collapse of a polymer with $N = 724$ at $T_q = 1$. The data at early times $t \leq 10^5$ indeed shows that the behavior is consistent with an expanded coil with an exponent equal to the Flory exponent $\nu_F = 3/5$. This consolidates the foundation of the relation (36) provided t_w is at early times. Now at the observation time t there could be two possibilities. Firstly, if t is late enough, then we expect that all the monomers will be inside a cluster which gives $R_g \sim C_s^{1/d}$ so that $\rho(t) = 1$. Thus considering the maximum overlap between $\rho(t)$ and $\rho(t_w)$ we get

$$C(t, t_w) \sim C_s^{-(\nu_F d-1)}. \tag{37}$$

This gives the lower bound. Secondly, with the assumption that the polymer still is in an expanded state even at time t, then $\rho(t) = \rho(t_w)$ holds and we obtain

$$C(t, t_w) \sim C_s^{-2(\nu_F d-1)}, \tag{38}$$

providing the upper bound for the aging exponent λ_c. Thus by combining (37) and (38) we arrive at the bounds

$$(\nu_F d - 1) \leq \lambda_c \leq 2(\nu_F d - 1). \tag{39}$$

Putting $\nu_F = 3/5$ in (39) one would get $4/5 \leq \lambda_c \leq 8/5$. Further, inserting the more precise numerical estimate $\nu = 0.587597$,[71] we get

$$0.762791 \leq \lambda_c \leq 1.525582. \tag{40}$$

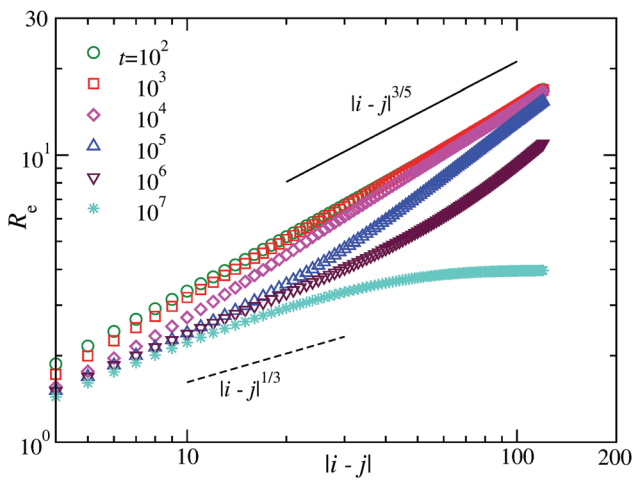

Fig. 15 Geometrical distance between monomers i and j which are at a distance $|i-j|$ along the contour of the chain for a polymer with $N = 724$ at different times during collapse at $T_q = 1$. The solid line shows the expected behavior for an extended coil and the dashed line shows the behavior in the collapsed phase.

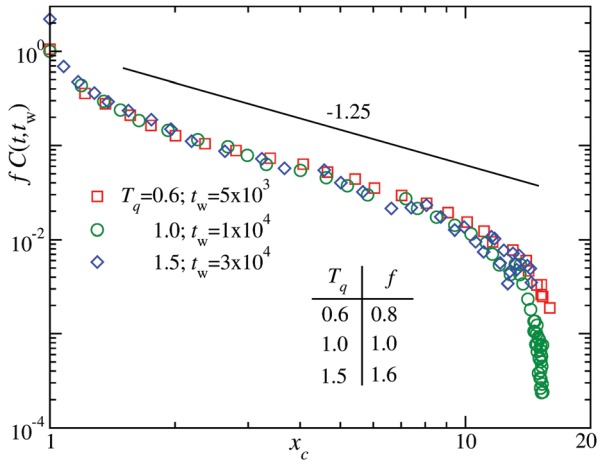

Fig. 16 Plots to show the temperature independent scaling of the autocorrelation function $C(t,t_w)$ with respect to $x_c = C_s(t)/C_s(t_w)$. Note that to obtain the data collapse, the values of $C(t,t_w)$ in each case are multiplied by a factor f that provides the ratio of the amplitudes A_c at different T_q. The solid line there again shows the power-law behavior (34) with an exponent $\lambda_c = 1.25$.

The validity of this bound can also be readily verified from the consistency of our data in Fig. 14 with the solid line having the power-law decay with exponent 1.25. We make the choice $t_w \leq 10^5$ in all the plots so that the assumption that at time t_w the polymer is in an expanded state is valid. This choice can also be appreciated from the plots in Fig. 15 where it is evident that the expanded coil behavior ($R_e \sim |i-j|^{3/5}$) is gradually changing after $t = 10^5$ to the behavior expected for the collapsed phase, $R_e \sim |i-j|^{1/d}$ with $d = 3$ here. The little off behavior of the data for $t_w = 10^5$ in Fig. 14 is indeed due to the fact that at $t = 10^5$ the formation of stable clusters has already initiated to change the coiled behavior of the chain. A more precise estimate of λ_c based on a FSS analysis is presented elsewhere.[12]

Finally we verify the effect of quench temperature T_q on the scaling of the autocorrelation functions. In Fig. 16 we plot $C(t,t_w)$ *vs.* x_c at different T_q. The y-axis has been multiplied by a factor $f = A_c(T_q = 1)/A_c(T_q)$ to collapse them onto a single master curve, similar to the non-universal metric factor in Fig. 11. The values of f used are quoted in the figure and seem to be similar to the metric factors (f_s) used in the scaling analyses for the cluster growth. The resulting master curve is nicely following the expected behavior (34) with the exponent $\lambda_c = 1.25$ as shown by the solid line. This demonstrates that the power-law scaling and the corresponding theoretical bounds predicted for the decay exponent λ_c are rather independent of the temperature T_q.

5 Conclusion

We have presented a comprehensive study on the dynamics of the collapse transition in a homopolymer model *via* Monte Carlo simulations. For the sake of completeness using the sophisticated multicanonical technique we have acquired the equilibrium finite-size scaling of our model. Importantly, we have obtained the behavior over the full temperature range of the model as well as the finite-size theta transition or collapse transition temperature $T_\theta(N)$. This knowledge eased the task of choosing an appropriate range of temperatures for understanding the kinetics of collapse.

Our results from dynamic Monte Carlo simulations, which mimic diffusive transport, apparently show the Rouse behavior, verified from the scaling of the collapse time with respect to the polymer length. Although the asymptotic behavior suggests a linear scaling. Particular focus in this work has been on the nonequilibrium evolution dynamics of a chain after a quench into the globular phase from an expanded coil state. We have shown that this occurs *via* the formation and growth of clusters of monomers which eventually coarsen or coalesce with each other before finally getting accumulated to a single cluster forming the globule. By disentangling the initial cluster-formation stage from the cluster-coarsening stage, we show that initially the cluster formation occurs rather slowly with $C_s(t) \sim t^{1/3}$ before crossing over to a faster linear growth in the coarsening stage.

Regarding the kinetics of the collapse we have paid much of our attention to find out the scaling law related to the growth of clusters in the coarsening stage. By drawing the analogy with well known coarsening phenomena for the Ising model[26] we found scaling in the cluster-size distribution functions as well as in the cluster growth. For the estimation of the exponent related to the cluster growth we have shown how usual methods may lead to misleading values. Due to the presence of an initial cluster-formation stage, the introduction of a crossover cluster size in the scaling ansatz and the corresponding nonequilibrium finite-size scaling analysis of our numerical results reveals a nearly linear growth law contradicting the very few existing studies.[21–23] While a decrease in the quench temperature (which mimics the solvent quality) results in a faster collapse of the chain, the linear scaling of the cluster growth remains unaltered and is associated with the presence of a universal finite-size scaling function.

In addition to single-time quantities, we have investigated a two-time property during the collapse which probes another important aspect of nonequilibrium processes, *i.e.*, aging. By exploiting the cluster identification technique we have constructed a suitable two-time autocorrelation function analogous to the usual density–density autocorrelation. The presence of aging is evident from the absence of time-translational invariance in the behavior of such autocorrelation functions for different waiting times. More importantly we have observed the presence of a dynamic power-law scaling as $C(t,t_w) \sim [C_s(t)/C_s(t_w)]^{-\lambda_c}$ with the related dynamic aging exponent $\lambda_c = 1.25$. We have provided simple theoretical arguments supported by our numerical results to predict the bound $(\nu_F d - 1) \leq \lambda_c \leq 2(\nu_F d - 1)$ involving the universal Flory exponent ν_F. Our numerical results show that the bound is strictly obeyed and λ_c is independent of the quench temperature.

The methods presented in this work are simple and could be of general validity. They should find application in more complex situations. In particular, the coil-globule or collapse transition of a polymer bears strong connection with conformational transitions observed in many biomolecules, *e.g.*, proteins. Proteins are

heteropolymers and therefore should also exhibit a similar coil-globule transition. An unfolded protein is often considered to be a highly expanded coil. Upon transfering from a strongly denaturing condition to a native condition it undergoes a conformational transition to form a folded (compact) structure. In doing so the protein molecule experiences a hydrophobic collapse which is pretty similar to the homopolymer collapse transition. It has been observed in experiments[3–5] *via* small angle X-ray scattering and single molecule fluorescence spectroscopy, as well as in simulations[6] that such a collapse precedes the folding of proteins. The collapse reduces its configurational entropy, which in turn facilitates the actual folding process.[72] Of course, simultaneous occurrence of the collapse and folding cannot be ruled out. Hence, considering this close connection, a better understanding of the collapse in polymers shall open up opportunities to shed some new light on the folding process of proteins, particularly in the kinetics perspective. As a first step in this regard, a study of the collapse kinetics of a heteropolymer is in progress.[73]

Finally, we feel that even though hydrodynamic or solvent effects are in general important, the Monte Carlo dynamics used in our simulation should provide a qualitative picture for many realistic situations. Experiments on polymers in constrained environment, *e.g.*, polymers adsorbed on a fluid surface (that resembles lipid-membranes of cells)[74,75] show negligible hydrodynamic effects. Furthermore, recent successful experiments on isolated polymers in vacuum[76–78] should encourage direct experimental verification of the results presented here. Still it would definitely be interesting to test the validity of the scaling laws presented in this work in presence of hydrodynamic interaction by doing molecular dynamics simulations which we take as a future endeavor. In this context one must expect that the clusters formed during the collapse exhibit a Brownian motion until they collide with each other to grow in size. This has been observed in case of droplet condensation in the vapor-liquid transition close to the co-existence curve[79] where the observed growth exponent has the same value as the Lifshitz–Slyozov exponent but the underlying mechanism is entirely different.[80,81] For a polymer, the internal constraint of connectivities between the individual clusters may play a significant role in controlling such motion. However, presence of such Brownian motion of the clusters aided by hydrodynamic flow can be ruled out in the results presented here. In fact, in equilibrium studies it has been shown that diffusion of the collapsed chain (single cluster) in absence of hydrodynamics is rather anomalous in nature[82] and is reminiscent of a slow glass-like dynamics.

Acknowledgements

The project was funded by the European Union and the Free State of Saxony, the Collaborative Research Centre SFB/TRR 102 (project B04), the Deutsche Forschungsgemeinschaft (DFG) under Grant No. JA 483/24-3 and JA 483/31-1, the Leipzig Graduate School of Natural Sciences ''BuildMoNa'', and the Deutsch-Französische Hochschule (DFH-UFA) through the Doctoral College ''$\mathbb{L}^4$'' under Grant No. CDFA-02-07, and further supported by the EU Marie Curie IRSES network DIONICOS under Contract No. PIRSES-GA-2013-612707.

References

1 W. H. Stockmayer, *Macromol. Chem. Phys.*, 1960, **35**, 54–74.
2 I. Nishio, S. T. Sun, G. Swislow and T. Tanaka, *Nature*, 1979, **280**, 208–209.
3 L. Pollack, M. W. Tate, A. C. Finnefrock, C. Kalidas, S. Trotter, N. C. Darnton, L. Lurio, R. H. Austin, C. A. Batt, S. M. Gruner and S. G. J. Mochrie, *Phys. Rev. Lett.*, 2001, **86**, 4962–4965.
4 M. Sadqi, L. J. Lapidus and V. Muñoz, *Proc. Natl. Acad. Sci. U. S. A.*, 2003, **100**, 12117–12122.
5 B. Schuler, E. A. Lipman and W. A. Eaton, *Nature*, 2002, **419**, 743–747.
6 C. J. Camacho and D. Thirumalai, *Proc. Natl. Acad. Sci. U. S. A.*, 1993, **90**, 6369–6372.
7 P.-G. de Gennes, *Scaling Concepts in Polymer Physics*, Cornell University Press, Ithaca, New York, 1979.
8 M. Doi and S. F. Edwards, *The Theory of Polymer Dynamics*, Clarendon, Oxford, 1986.
9 J. des Cloizeaux and G. Jannink, *Polymers in Solution*, Clarendon, Oxford, 1990.
10 S. Majumder and W. Janke, *Europhys. Lett.*, 2015, **110**, 58001.
11 G. Bunin and M. Kardar, *Phys. Rev. Lett.*, 2015, **115**, 088303.
12 S. Majumder and W. Janke, *Phys. Rev. E: Stat., Nonlinear, Soft Matter Phys.*, 2016, **93**, 032506.
13 N. Kamerlin and C. Elvingson, *Macromolecules*, 2016, **49**, 5740–5749.
14 Z. Wang, J. Yu and B. Chu, *Macromolecules*, 1992, **25**, 1618–1620.
15 Q. Ying, B. Chu and A. Yu. Grosberg, *Macromolecules*, 1995, **28**, 180–189.
16 P. W. Zhu and D. H. Napper, *J. Chem. Phys.*, 1997, **106**, 6492–6498.
17 J. Xu, J. Zhu, S. Luo, C. Wu and S. Liu, *Phys. Rev. Lett.*, 2006, **96**, 027802.
18 A. J. Bray, *Adv. Phys.*, 2002, **51**, 481–587.
19 ed. S. Puri and V. Wadhawan, *Kinetics of Phase Transitions*, CRC Press, Boca Raton, 2009.
20 P.-G. de Gennes, *J. Phys., Lett.*, 1985, **46**, 639–642.
21 Yu. A. Kuznetsov, E. G. Timoshenko and K. A. Dawson, *J. Chem. Phys.*, 1996, **104**, 3338–3347.
22 A. Byrne, P. Kiernan, D. Green and K. A. Dawson, *J. Chem. Phys.*, 1995, **102**, 573–577.
23 Yu. A. Kuznetsov, E. G. Timoshenko and K. A. Dawson, *J. Chem. Phys.*, 1995, **103**, 4807–4818.
24 A. Halperin and P. Goldbart, *Phys. Rev. E: Stat. Phys., Plasmas, Fluids, Relat. Interdiscip. Top.*, 2000, **61**, 565–573.
25 J. Schmelzer and F. Schweitzer, *J. Non-Equilib. Thermodyn.*, 1997, **12**, 255–270.
26 S. Majumder and S. K. Das, *Phys. Rev. E: Stat., Nonlinear, Soft Matter Phys.*, 2010, **81**, 050102(R); S. Majumder and

S. K. Das, *Phys. Rev. E: Stat., Nonlinear, Soft Matter Phys.*, 2011, **84**, 021110; S. Majumder and S. K. Das, *Phys. Chem. Chem. Phys.*, 2013, **15**, 13209–13218.
27 I. M. Lifshitz and V. V. Slyozov, *J. Phys. Chem. Solids*, 1961, **19**, 35–50.
28 M. Zannetti, *Aging in domain growth*, in ref. 19, pp. 153–202.
29 M. Henkel and M. Pleimling, *Non-Equilibrium Phase Transitions*, Ageing and Dynamical Scaling far from Equilibrium, Springer, Heidelberg, 2010, vol. 2.
30 D. S. Fisher and D. A. Huse, *Phys. Rev. B: Condens. Matter Mater. Phys.*, 1988, **38**, 373–385.
31 F. Liu and G. F. Mazenko, *Phys. Rev. B: Condens. Matter Mater. Phys.*, 1991, **44**, 9185–9191.
32 J. Midya, S. Majumder and S. K. Das, *J. Phys.: Condens. Matter*, 2014, **26**, 452202.
33 M. Henkel, A. Picone and M. Pleimling, *Europhys. Lett.*, 2004, **68**, 191–197.
34 E. Lorenz and W. Janke, *Europhys. Lett.*, 2007, **77**, 10003.
35 N. V. Dokholyan, E. Pitard, S. V. Buldyrev and H. E. Stanley, *Phys. Rev. E: Stat., Nonlinear, Soft Matter Phys.*, 2002, **65**, 030801(R).
36 E. Pitard and J.-P. Bouchaud, *Eur. Phys. J. E: Soft Matter Biol. Phys.*, 2001, **5**, 133–148.
37 A. Milchev, A. Bhattacharaya and K. Binder, *Macromolecules*, 2001, **34**, 1881–1893.
38 J. Zierenberg and W. Janke, *Europhys. Lett.*, 2015, **109**, 28002.
39 B. A. Berg and T. Neuhaus, *Phys. Lett. B*, 1991, **267**, 249–253; B. A. Berg and T. Neuhaus, *Phys. Rev. Lett.*, 1992, **68**, 9–12.
40 W. Janke, *Int. J. Mod. Phys. C*, 1992, **03**, 1137–1146; W. Janke, *Physica A*, 1998, **254**, 164–178.
41 W. Janke and W. Paul, *Soft Matter*, 2016, **12**, 642–657.
42 W. Janke, Histograms and all that, invited lecture, in *Computer Simulations of Surfaces and Interfaces*, ed. B. Dünweg, D. P. Landau and A. I. Milchev, NATO ScienceSeries, II. Mathematics, Physics and Chemistry, Kluwer, Dordrecht, 2003, vol. 114, pp. 137–157.
43 J. Zierenberg, M. Marenz and W. Janke, *Comput. Phys. Commun.*, 2013, **184**, 1155–1160.
44 W. Janke, Monte Carlo Simulations in Statistical Physics – From Basic Principles to Advanced Applications, in *Order, Disorder and Criticality: Advanced Problems of Phase Transition Theory*, ed. Y. Holovatch, World Scientific, Singapore, 2012, vol. 3, pp. 93–166.
45 S. Schnabel, W. Janke and M. Bachmann, *J. Comput. Phys.*, 2011, **230**, 4454–4465.
46 B. Efron, *The Jackknife, the Bootstrap, and Other Resampling Plans*, Society for Industrial and Applied Mathematics, Philadelphia, PA, 1982.
47 B. Efron and R. J. Tibshirani, *An Introduction to the Bootstrap*, Springer Science+Business Media, Dordrecht, 1994.
48 D. P. Landau and K. Binder, *A Guide to Monte Carlo Simulations in Statistical Physics*, Cambridge University Press, Cambridge, 2005.
49 P. E. Rouse, *J. Chem. Phys.*, 1953, **21**, 1272–1280.
50 W. Paul, T. Strauch, F. Rampf and K. Binder, *Phys. Rev. E: Stat., Nonlinear, Soft Matter Phys.*, 2007, **75**, 060801.
51 T. Vogel, M. Bachmann and W. Janke, *Phys. Rev. E: Stat., Nonlinear, Soft Matter Phys.*, 2007, **76**, 061803.
52 D. F. Parsons and D. R. Williams, *Phys. Rev. E: Stat., Nonlinear, Soft Matter Phys.*, 2006, **74**, 041804.
53 D. F. Parsons and D. R. Williams, *J. Chem. Phys.*, 2006, **124**, 221103.
54 D. Seaton, T. Wüst and D. P. Landau, *Phys. Rev. E: Stat., Nonlinear, Soft Matter Phys.*, 2010, **81**, 011802.
55 J. Zierenberg, M. Marenz and W. Janke, *Polymers*, 2016, **8**, 333.
56 S. Schnabel, M. Bachmann and W. Janke, *J. Chem. Phys.*, 2009, **131**, 124904.
57 J. Gross, T. Neuhaus, T. Vogel and M. Bachmann, *J. Chem. Phys.*, 2013, **138**, 074905.
58 C. F. Abrams, N.-K. Lee and S. P. Obukhov, *Europhys. Lett.*, 2002, **59**, 391–397.
59 N. Kikuchi, J. F. Ryder, C. M. Pooley and J. Yeomans, *Phys. Rev. E: Stat., Nonlinear, Soft Matter Phys.*, 2005, **71**, 061804.
60 D. A. Huse, *Phys. Rev. B: Condens. Matter Mater. Phys.*, 1986, **34**, 7845–7850.
61 B. Otrovsky and Y. Bar-Yam, *Biophys. J.*, 1995, **68**, 1694–1698.
62 H. Nagel and W. Janke, *Phys. Rev. E: Stat., Nonlinear, Soft Matter Phys.*, 2016, **93**, 052112.
63 M. E. Fisher, The theory of critical point singularities, in *Critical Phenomena*, ed. M. S. Green, Proc. 51st Enrico Fermi Summer School, Varenna, Italy, Academic Press, London, 1971, pp. 1–99.
64 ed. V. Privman, *Finite Size Scaling and the Numerical Simulations of Statistical Systems*, World Scientific, Singapore, 1990.
65 S. K. Das, S. Roy, S. Majumder and S. Ahmad, *Europhys. Lett.*, 2012, **97**, 66006.
66 J. M. Polson and M. J. Zuckermann, *J. Chem. Phys.*, 2002, **116**, 7244–7254.
67 V. Privman and M. E. Fisher, *Phys. Rev. B: Condens. Matter Mater. Phys.*, 1984, **30**, 322–327.
68 C.-K. Hu, C.-Y. Lin and J.-A. Chen, *Phys. Rev. Lett.*, 1995, **75**, 193–196.
69 R. Paul, G. Schehr and H. Rieger, *Phys. Rev. E: Stat., Nonlinear, Soft Matter Phys.*, 2007, **75**, 030104(R).
70 J. Midya, S. Majumder and S. K. Das, *Phys. Rev. E: Stat., Nonlinear, Soft Matter Phys.*, 2015, **92**, 022124.
71 N. Clisby, *Phys. Rev. Lett.*, 2010, **104**, 055702.
72 G. Haran, *Curr. Opin. Struct. Biol.*, 2012, **22**, 14–20.
73 S. Majumder and W. Janke, in progress.
74 B. Maier and J. O. Rädler, *Phys. Rev. Lett.*, 1999, **82**, 1911–1914.
75 B. Maier and J. O. Rädler, *Macromolecules*, 2000, **33**, 7185–7194.
76 M. Tress, E. U. Mapesa, W. Kossack, W. K. Kipnusu, M. Reiche and F. Kremer, *Science*, 2013, **341**, 1371–1374.
77 S. Förster and W. Widdra, *J. Chem. Phys.*, 2014, **141**, 054713.
78 S. Förster, E. Kohl, M. Ivanov, J. Gross, W. Widdra and W. Janke, *J. Chem. Phys.*, 2014, **141**, 164701.
79 S. Roy and S. K. Das, *Soft Matter*, 2013, **9**, 4178–4187.
80 K. Binder and D. Stauffer, *Phys. Rev. Lett.*, 1974, **33**, 1006–1009.
81 E. D. Siggia, *Phys. Rev. A: At., Mol., Opt. Phys.*, 1979, **20**, 595–605.
82 A. Milchev and K. Binder, *Europhys. Lett.*, 1994, **26**, 671–676.

